doi: 10.82124/CEAS-GNC-2026-047 CEAS-GNC-2026-047

Development and Validation of Enabling Guidance and Control Technologies for Smart Launchers

João P. Belfo GNC Engineer, DEIMOS Engenharia SA, GNC/AOCS Competence Center, 1070-061, Lisbon, Portugal. jpbelfo@indracompany.com

Pedro Guerreiro GNC Engineer, DEIMOS Engenharia SA, GNC/AOCS Competence Center, 1070-061, Lisbon, Portugal. pmguerreiro@indracompany.com

Bruno Ribeiro GNC Engineer, DEIMOS Engenharia SA, GNC/AOCS Competence Center, 1070-061, Lisbon, Portugal. baribeiro@indracompany.com

Afonso Botelho GNC Engineer, DEIMOS Engenharia SA, GNC/AOCS Competence Center, 1070-061, Lisbon, Portugal. adbotelho@indracompany.com

G. Videira GNC Engineer, DEIMOS Engenharia SA, GNC/AOCS Competence Center, 1070-061, Lisbon, Portugal. gvideira@indracompany.com

J. Vasconcelos Head of GNC/AOCS Competence Center, DEIMOS Engenharia SA, 1070-061, Lisbon, Portugal. jmvasconcelos@indracompany.com

P. Rosa Head of Flight Segment, DEIMOS Engenharia SA, 1070-061, Lisbon, Portugal. parosa@indracompany.com

Adolfo D. Silva System Engineer, Orbex Space, UK. adolfo.dasilva@orbex.space

Aitor R. Gomez Postdoc, Section of Automation & Control, Aalborg University, Aalborg, Denmark. arg@es.aau.dk

Jakob Stoustrup Professor, Section of Automation & Control, Aalborg University, Aalborg, Denmark. jakob@es.aau.dk

P. Simplício GNC Engineer, European Space Agency, ESTEC, Noordwijk, The Netherlands. pedro.simplicio@esa.int

M. Casasco Head of GNC Systems Architecture Section, European Space Agency, ESTEC, Noordwijk, The Netherlands. massimo.casasco@esa.int

ABSTRACT

The project SURE (Smart Launchers – Autonomous MVM and Monitoring Systems for Safe and Adaptable GNC System) focused on the development of smart launcher enabling technologies that pave the way for improved launcher robustness, reliability, safety and commercial application. This paper presents three innovative solutions derived in the project, in the areas of Guidance, Robust Control, and Safety, describing the principles of each one and highlighting the results achieved in high-fidelity validation, with a higher focus on the guidance topic. The real-time optimized guidance allows a launcher to autonomously update its trajectory, based on a tailored first-order solver xPIPG, shown to be computationally more efficient than the standard ECOS. A robust control architecture with a wind disturbance observer and a load relief controller is shown to successfully minimize the load and the drift rate error, allowing for wider launch windows, with a solution that relies only on an engineering design that does not require any additional sensor or other hardware. A robust safety control methodology is also

presented, employing Control Barrier Functions, ensuring that the vehicle remains within drift bounds and attitude errors. The proposed technologies are validated in high-fidelity Model-in-the-Loop (MIL) and also Software-in-the-Loop (SIL), achieving a high degree of representativity and suitability for future adoption in real applications. Additional developments, such as estimation of flexible modes, are also proposed.

Keywords: Safe and Adaptable GNC, Smart Launcher, Onboard Guidance, Robust Wind Observer, Load Relief, Safety Filter, Control Barrier Function

Nomenclature

CBF	=	Control Barrier Function
ECOS	=	Embedded Conic Solver
FBG	=	Fiber Bragg Gatting
GNC	=	Guidance, Navigation and Control
MC	=	Monte Carlo
MCI	=	Mass, Centre of mass and Inertia
MIL	=	Model-in-the-loop
SCvx	=	Successive Convexification
SIL	=	Software-in-the-loop
SLE	=	Smart Launcher Enabler
TRL	=	Technology Readiness Level
V&V	=	Verification and Validation
xPIPG	=	Extrapolated Proportional-Integral Projected Gradient
WDO	=	Wind Disturbance Observer

1 Introduction

Europe has a consolidated know-how in access to space and is experiencing considerable growth in this market. New systems are already available or are going to be available in the near future (e.g. VEGA-C, Ariane 6), and others are currently under development by several actors (e.g. Orbex Prime). An increase in the launch rate and a decrease in launch costs is necessary to maintain competitiveness in a growing access-to-space market where new solutions are constantly proposed and introduced. To do so, it is necessary to increase the capability of the launcher to deal with engineering challenges that drive the preparation and the V&V of each launch mission, such as:

- Sensitivity to day-of-flight wind and weather conditions.
- Adaptive flight programs for increased responsiveness.
- Stringent load relief requirements due to lighter and more flexible structural designs.
- Stringent and variable safety constraints and flight corridors (e.g. mission-dependent or launch site-dependent stage fall-down and no-fly zones).
- Safe operations and equipment/elements life extending requirements, also related with the goal of achieving (partial) reusability.

Therefore, a paradigm shift is needed in which autonomous functionalities onboard are necessary to address the aforementioned challenges in a more efficient and safe manner. To address these issues, the SURE activity [1] was created, for which the Consortium is composed of:

- Deimos Engenharia S.A. (Indra, Portugal), as prime contractor.
- Deimos Space UK Ltd (Indra, United Kingdom).

- Orbital Express Launch Ltd. (Orbex, United Kingdom).
- Aalborg Universitet (AAU, Denmark).

This paper addresses the development of innovative Smart Launcher Enabling (SLE) technologies, with a higher focus on Real-time optimized guidance and the preliminary study related with the application of strain sensors for flexible states estimation and their control feedback.

The objectives of the project are presented in Section 2, providing an overview of the motivations for the SLEs and the adopted scenarios. It is shown that these are highly relevant problem areas for the next-generation launchers, and the scenarios illustrate the benefits of the explored techniques. Within the same section, the selection of the SLEs and the scenarios are described, together with a justification of the relevance of the considered problems.

Section 3 describes the following techniques and presents the corresponding results:

- **Real-Time Optimized Guidance** for a computationally efficient on-line recomputation of the trajectory. A new solver (xPIPG [6]) is proposed and the benefits in terms of convergence and execution time are demonstrated.
- **Robust Control using Wind Information** with the goal of reducing wind-induced load. The improvement in performance is demonstrated, highlighting the benefits of a control architecture that properly exploits the segmentation in a feedback controller, a flexible filter and a load relief controller, without the need of any additional hardware.
- **Robust Safety Control**, that adopts Control Barrier Functions (CBFs) which achieve safety by design, both in position and attitude. The adopted solution is able to reduce the standard V&V effort and provide a priori confidence of the controller safety.
- **Robust Control with Feedback of Flexible States estimated via Strain Sensors,** where the control architecture is augmented with the flexible states, yielding improved attitude control performance.

2 Project Objectives and SLE Definition

The overall objectives of the SURE project are as follows:

Goal 1: Identify and select the most promising and innovative Smart Launcher Enabler (SLE) technologies. This was accomplished by performing a thorough state-of-the-art (SOTA) review followed by a selection of the most promising solutions using a list of pre-defined selection criteria.

Goal 2: Design and develop autonomous GNC methods and tools based on the selected SLEs. To accomplish this, the techniques identified and selected previously are evaluated during a first preliminary design step, i.e., proof-of-concept, and a second step, i.e., detailed design.

Goal 3: Demonstrate the adequacy of the developed SLEs via Model-In-the-Loop (MIL) and Software-In-the-Loop (SIL) testing, allowing the techniques to reach TRL 4.

Goal 4: Define future work and roadmap for the maturation and further development of the SLEs, by identifying and consolidating a list of priorities, strengths, shortcomings and recommendations for research and development in the next 5 years.

2.1 Selection of SLEs

The selection process was carried out in two different levels: first, the **techniques associated to each SLE**, obtained during the thorough state-of-the-art review, were evaluated against criteria that are more specific to the SLE topic; subsequently, the **SLE topics were selected** based on the indicators 1) and 2)

mentioned in the Goal 1 described above, yielding a group of **3 SLEs, out of a total of 11 SLEs, with one technique per SLE**. These SLEs are:

- **SLE 1 – Real-Time Optimized Guidance**: addresses the Successive Convexification sub-problem by considering a first order solver named Extrapolated Proportional-Integral Projected Gradient (xPIPG), and compare its performance to the one of ECOS, a state-of-practice second order solver. As mentioned in the sequel, this SLE innovation comes from the fact that xPIPG can perform faster than ECOS and, given its simplicity, allows for an easier V&V process.
- **SLE 4 - Control using Wind Information**: addresses the problem of load relief by introducing the Wind Disturbance Observer (WDO) element, designed with robust H_∞ techniques, in the controller architecture. The WDO estimates the wind perturbation which is then feedbacked via a proportional gain to reduce the wind-induced load. As will be observed, the approach adopted leads to significant load reduction while maintaining robustness and a high level of modularity.
- **SLE 11 - Robust Safety Control**: addresses the problem of autonomous safety in the context of a launch vehicle by developing a Safety Filter incorporated in the control architecture and based on Control Barrier Functions (CBFs). The Safety Filter designed, which is active when needed, allows to significantly reduce deviation from the reference trajectory, contributing to a safer flight envelope.

2.2 Reference scenarios

The SURE project considers two different scenarios:

1. **Ascent flight scenario:** launcher model with parameters provided by Orbex (see figure 1), a member of the SURE Consortium. The scenario counts with high-fidelity models of aerodynamic, MCI, propulsion, wind and turbulence, flexible and sloshing dynamics, including the reference trajectory with the Sutherland spaceport as launch site. The guidance considered is a lookup-table providing the reference trajectory. The navigation corresponds to a performance model obtained with the Navigation solution of Indra Deimos used in several other projects, based on the extended Kalman filter (EKF) and the use of IMU and GNSS.
2. **Descent flight scenario:** launch model from RETALT mission [2]. This scenario considers high-fidelity models of aerodynamics, MCI, propulsion, RCS, Flaps and wind, including the RETALT Guidance (see figure 2) and Controller as baseline.

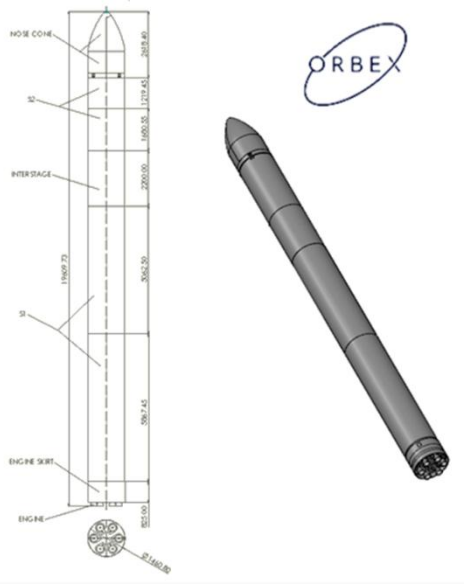

Fig. 1: Launch vehicle considered for Ascent scenario

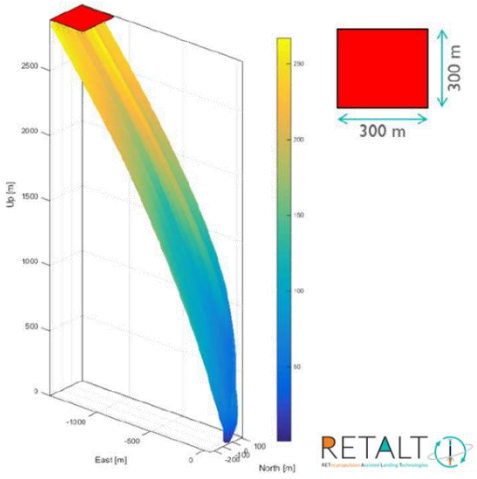

Fig. 2: RETALT landing phase

Both scenarios were implemented through the ESA-i4GNC framework, a tool developed

fully by Indra Deimos during the AI4GNC project [3].

3 Smart Launcher Enablers Development and Results

This section provides an overview of the techniques developed under each SLE and the main results obtained, focusing on the main advantages and disadvantages of the techniques and highlighting the consortium's recommendations and proposed future work. As mentioned before, this section focuses mainly on the SLE 1 developments, and the preliminary study related to the application of strain sensors to estimate flexible states and the control design of their feedback. More information about SLE 4 and 11 can be found in [8] and [10].

3.1 Real-Time Optimized Guidance

SLE 1 is related with **real-time onboard optimized guidance** solutions to allow the Smart Launcher to **autonomously compute** or **update its trajectory**. The technique selected within SLE 1 is based on the **Successive Convexification** (SCvx) solution which tackles the problem of solving a nonlinear optimization problem by iteratively linearizing the dynamics, yielding a convex sub-problem at each iteration, for which fast convex solvers can be used [4]. In particular, the **first order xPIPG solver [6] has been applied** to the **powered descent landing guidance** problem based on the **RETALT vehicle** benchmark and **compared to a state-of-practice solver** named Embedded Conic Solver (**ECOS) [7]**.

Going more into mathematical detail, each sub-problem is convexified about the state/control profiles and final time obtained in the previous SCvx iteration, denoted as $(\bar{x}_k, \bar{u}_k, \bar{t}_f)$. To overcome artificial infeasibility, virtual controls ν_k are included for the v and (θ, ψ, T) states in the linearized dynamics, giving the formulation additional degrees-of-freedom with which to manoeuvre and ensure problem feasibility, and penalized quadratically in the cost function with the weight coefficient $w_{vc} > 0$ to discourage their use. A soft trust-region is also employed to avoid unboundedness, by penalizing quadratically the deviation of the optimization variables from $(\bar{x}_k, \bar{u}_k, \bar{t}_f)$ with the coefficients $(w_{tr,x}, w_{tr,u}, w_{tr,t_f}) > 0$. The dynamics are discretized with a mixed zero-order hold and Euler approach, yielding the SCvx sub-problem:

$$
\begin{aligned}
\underset{x_k, u_k, t_f, \nu_k}{\text{minimize}} \quad & \sum_{k=0}^{N-1} \left[w_T T_k + w_u \left(\dot{\theta}_k^{\,2} + \dot{\psi}_k^{\,2} \right) + w_{tr,u} \left\| u_k - \bar{u}_k \right\|_2^2 + w_{tr,x} \| x_k - \bar{x}_k \|_2^2 + w_{vc} \| \nu_k \|_2^2 \right] + w_{tf} t_f + w_{tr,t_f} \left\| t_f - \bar{t}_f \right\|_2^2 \\
\text{subject to} \quad & x_{k+1} = A_k x_k + B_k u_k + C_k t_f + E_k + S_{vc} \nu_k, \qquad k = 0, \ldots, N-1 \\
& x_0 = \bar{x}_0, S_f x_N = x_f \\
& \bar{\alpha}(x_k, u_k, t_f) \leq \alpha_{max} \\
& T_{\min} \leq T_k \leq T_{\max} \\
& \left| \dot{T}_k \right| \leq \dot{T}_{\max} \\
& \left| \dot{\theta}_k \right| \leq \dot{\theta}_{max}, \left| \dot{\psi}_k \right| \leq \dot{\psi}_{max} \\
& \left| \ddot{\theta}_k \right| \leq \ddot{\theta}_{max}, \left| \ddot{\psi}_k \right| \leq \ddot{\psi}_{max}
\end{aligned}
$$

where A_k, B_k, C_k, E_k model the linearized dynamics, S_{vc} is a selection matrix that assigns the virtual controls to the respective entries, and $\bar{\alpha}$ is the convexified and discretized aerodynamic angle-of-attack. Furthermore, constraints on the torque magnitude, on its derivative, on the angular rates and on the angular accelerations are also enforced.

Several improvements were made during the implementation of xPIPG, of which the most relevant are:

- **Initialization of SCvx algorithm:**

Three possibilities for the initial guess for the SCvx procedure were compared, namely:

- Linear State Interpolation **(LSI):** given by linearly interpolating the state $x = [r\ v\ m\ \theta\ \psi\ T]^T$ between its initial and final values and where the initial guess for the control is set to zero, i.e., $u = \left[\dot{\theta}\ \dot{\psi}\ \dot{T}\right] = 0$.
- Polynomial State Interpolation **(PSI)**: obtained by using information of the state time derivatives (more details below).
- Nominal Optimal Solution **(NOS)**: the optimal state/control profiles are obtained from applying the SCvx algorithm to the RETALT nominal mission setup.

The PSI initialization has the following features:

- Position and velocity are obtained by integration of a quadratic acceleration profile and satisfying initial and final conditions.

$$\begin{cases} a(t) = C_0 + C_1 t + C_2 t^2, \\ v(t) = v_0 + C_0 t + \frac{1}{2} C_1 t^2 + \frac{1}{3} C_2 t^3, \\ r(t) = r_0 + v_0 t + \frac{1}{2} C_0 t^2 + \frac{1}{6} C_1 t^3 + \frac{1}{12} C_2 t^4, \\ a(t_f) = a_f,\ v(t_f) = v_f,\ a(t_f) = a_f. \end{cases} \qquad \begin{cases} C_0 = a_f - \frac{6}{t_f}(v_f - v_0) + \frac{12}{t_f^2}(r_f - r_0 - \dot{r}_0 t_f), \\ C_1 = -\frac{6}{t_f} a_f + \frac{30}{t_f^2}(v_f - v_0) - \frac{48}{t_f^3}(r_f - r_0 - \dot{r}_0 t_f), \\ C_2 = \frac{6}{t_f^2} a_f - \frac{24}{t_f^3}(v_f - v_0) + \frac{36}{t_f^4}(r_f - r_0 - \dot{r}_0 t_f). \end{cases}$$

  with $a(t_f) = 0$.
- Yaw and pitch are linearly interpolated between initial and final conditions.
- Mass profile is computed assuming a thrust equal in magnitude to gravity force.
- Thrust profile is computed from thrust acceleration (computed such that the velocity propagation nonlinear dynamics holds exactly) divided by the mass coming from the aforementioned mass profile.

The obtained results showed that, when compared to LSI, PSI yields better running times while having similar optimality (final mass) and similar magnitude of dynamical constraints violations. Nevertheless, on top of that, NOS initialization showed a marginal gain with respect to PSI regarding runtime but a noticeable reduction on the number of SCvx rounds. Hence, as expected, NOS proved to be the best solution.

- **Warm start for the xPIPG of SCvx algorithm:**

Two methods for initializing the xPIPG convex solver regarding the estimates for the primal and dual variables were compared. These can be summarized as:

- **PrevSol**: initializes the convex solver with the solution of the previous SCvx round. For the first round, both primal and dual variables are set to zero.
- **ECQP**: initializes the convex solver with the solution to the Equality Constrained Quadratic Problem obtained from dropping out the inequality constraints in the SCvx sub-problem formulation shown above.

It was concluded that starting xPIPG with the previous solution (PrevSol) seems to be the best approach. PrevSol yields better runtimes while requiring a similar number of SCvx rounds. Another strength of PrevSol with respect to ECQP is the avoidance of any additional computation, since it relies on the readily available solution for the previous SCvx round, while ECQP needs to solve a linear system (KKT system).

- **Variable stopping criteria for the xPIPG convex solver**:

The main reason behind testing a variable stopping criteria for the convex solver used by the SCvx algorithm amounts to the observation that the first SCvx rounds do not need to be solved very accurately since they represent coarse approximations to the underlying non-convex optimization problem. In that regard, instead of solving all SCvx subproblems with a fixed/high precision, an approach with increasingly more precision/optimality is adopted as the subproblems better and better represent the original non-convex one close to a local (ideally global) optimum. For that reason, the implemented stopping criteria starts with high tolerances decreasing linearly until saturating at minimum values after a prescribed number of SCvx rounds.

- **Customized implementation**:

The most computationally heavy operations in xPIPG are the matrix multiplications of H^T and H at steps 3 and 4 of Algorithm 1 (see figure 3). In both steps, a matrix-vector multiplication is required where the matrix is very sparse, i.e., most elements are 0. The gradient term $\nabla f(\xi_i)$ would typically require a sparse matrix-vector multiplication as well, but the use of the Cholesky factorization-based preconditioning yields a diagonal uniform quadratic cost matrix, and thus it can be computed with a scalar-vector product instead.

Algorithm 1 xPIPG

Input $\rho \in [1, 2]$, ξ_0, η_0
Output z^*

1: $i = 0$
2: **while** stopping criteria is not met **do**
3: $\quad z_{i+1} = \pi_{\mathbb{D}}[\xi_i - \alpha_i(\nabla f(\xi_i) + H^T \eta_i)]$
4: $\quad w_{i+1} = \pi_{\mathbb{K}^\circ}[\eta_i + \beta_i(H(2z_{i+1} - \xi_i) - g)]$
5: $\quad \xi_{i+1} = (1 - \rho)\xi_i + \rho z_{i+1}$
6: $\quad \eta_{i+1} = (1 - \rho)\eta_i + \rho w_{i+1}$
7: $\quad i = i + 1$
8: **end while**

Fig. 3: xPIPG convex solver algorithm

Previously, a compressed sparse column (CSC) sparse matrix representation of H was used, which had already a far smaller computational burden in comparison to using dense matrices. However, the resulting matrix multiplication still has a significant computational overhead for iterating the indices of the non-zero entries. Therefore, in order to further improve the computational burden of the aforementioned steps, customized functions for the matrix-vector multiplications for the specific sparsity pattern of H were generated automatically using CasADi. CasADi is a software framework for numerical optimization and algorithmic differentiation. It provides efficient derivatives (gradients, Jacobians, and Hessians) of symbolic expressions, naturally supporting systems described by ordinary differential equations (ODEs) and DAEs.

With all the improvements addressed, it was possible to obtain the guidance metrics illustrated in figure 4, where it is possible to conclude that the xPIPG is able to significantly reduce the overall SCvx runtime required to compute an optimal and feasible trajectory. This reduction in runtime comes at the cost of a slight increase in the total number of SCvx rounds. Besides the reduction of the runtime when considering xPIPG over ECOS, another important advantage is the fact that the **convergence verification of xPIPG is easier to obtain** than ECOS since **xPIPG is a first order method.**

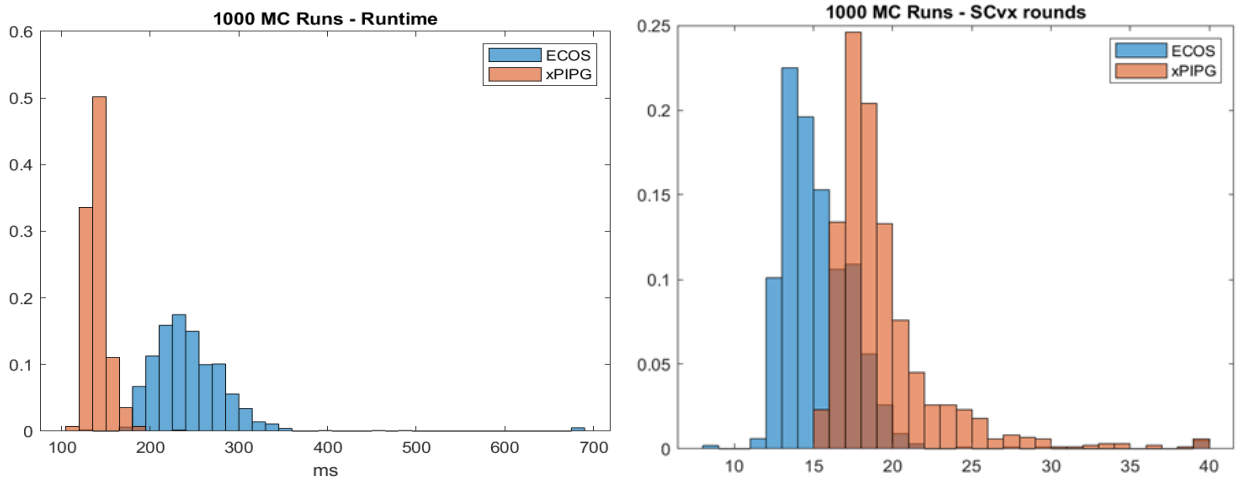

Fig. 4: Comparison of guidance metric between ECOS and xPIPG convex solvers

3.1.1 MIL – SIL Results

Following the implementation of the aforementioned features, the results shown below are obtained. In figure 5, it is possible to see a visual representation of 500 different reference trajectories computed through the described guidance algorithm. Even with dispersions in the initial conditions, 500 feasible trajectories that take the launcher to the landing site are obtained in a short time frame.

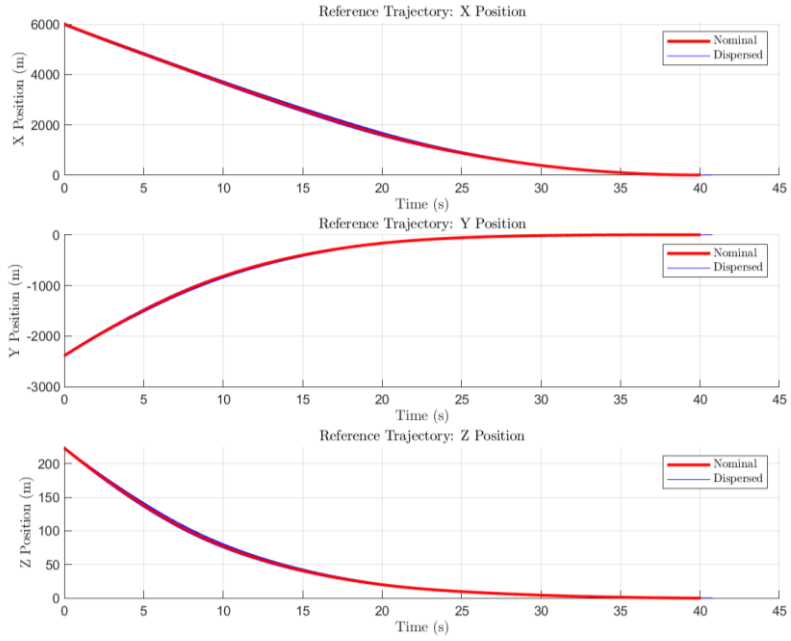

Fig. 5: Visual representation of 500 reference trajectories computed by the guidance algorithm

Furthermore, as displayed in figure 6, the combination of the guidance output and the landing controller achieves a high landing accuracy. The final deviations from the goal state are well within the requirements. At a final landing stage, the minimization of the velocity and attitude errors are prioritized by the controller over the minimization of the position error. However, as a trade-off, the velocity and the attitude channels show very good tracking performance.

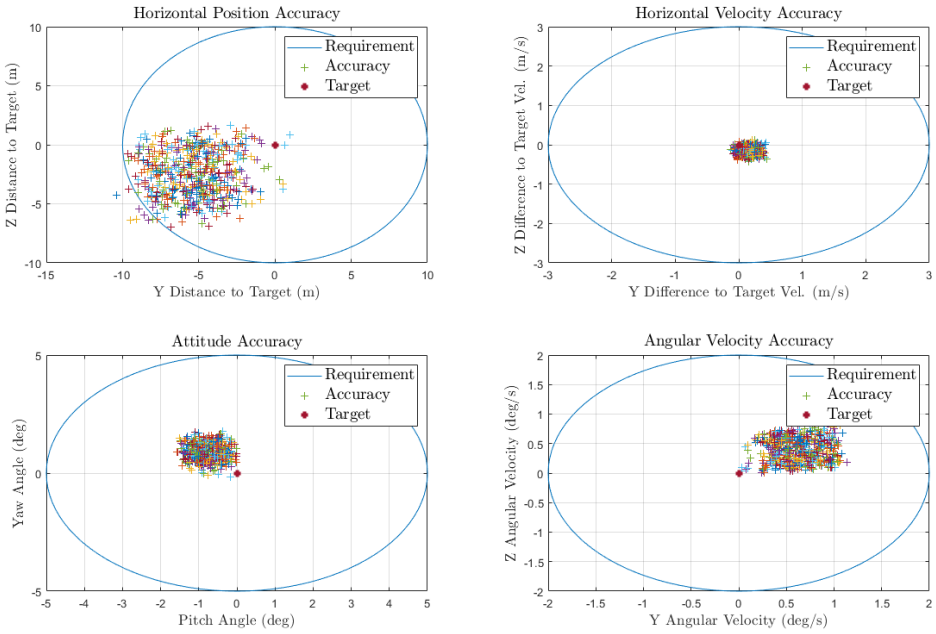

Fig. 6: Landing accuracy values for a MC simulation campaign with 500 shots

Additionally, figure 7 illustrates a comparison of the guidance metrics for a MC simulation with the guidance running in MIL and in SIL. As it is possible to see, running the guidance in SIL yields a significantly lower runtime than in MIL, while, since the guidance solution is the same, the SCvx rounds are equivalent.

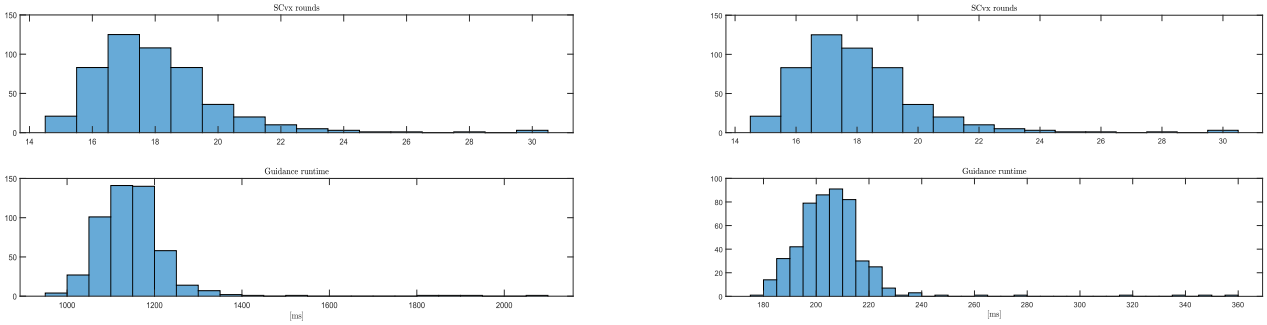

Fig. 7: Comparison of the guidance metrics for a MC simulation run in MIL (left) and SIL (right)

3.1.2 Conclusions

In summary, the impact of the outcomes of SLE 1 at system-level are as follows:

- **Reduced runtime.** As observed above, when compared to the state-of-the-art ECOS solver, xPIPG was able to decrease the average runtime from ~220 ms to 150 ms. **This reduction allows for a smaller delay** between the instant in which the solution is obtained (after SCvx converged) and the instant at which the SCvx initial conditions were retrieved. This delay can be viewed as the cost one needs to pay when using real-time optimized guidance.
- **With a reduced cost due to the developments in SLE 1**, one could **increase the number of trajectory re-computation during flight**, which may lead to a **higher landing accuracy**. At each trajectory re-computation, accumulated errors (deviations from the reference trajectory) are dealt with by considering the system's current state as boundary condition/problem constraint in the SCvx convex problem.

- **The efforts for Verification & Validation are reduced with a simpler SCvx convex solver**. First order methods such as xPIPG relying only on gradient evaluations and simple projection operations are much easier to understand and debug than second order/interior point methods like ECOS.
- Lower onboard processing requirements may allow its use on **smaller or more cost-constrained platforms**.

3.2 Control using Wind Information

SLE 4 tackles the topic of **reducing wind-induced load** experienced by the launcher vehicle by using wind information obtained by estimation during flight based on onboard measurements of typical quantities such as drift, attitude and their derivative estimations. Those quantities are then used by a Wind Disturbance Observer (WDO) which is designed based on robust H_∞ approach. This method has the main advantage of **not needing extra sensors** and, thus, it was adopted for SLE 4. Together with the WDO design, a **robust load relief controller** is also employed to **feedback the wind information** and, thus**, reduce the wind-induced load**. The ascent scenario was selected as a benchmark, which includes the first and second stage flight until the main engine cut-off (MECO) of a flexible vehicle.

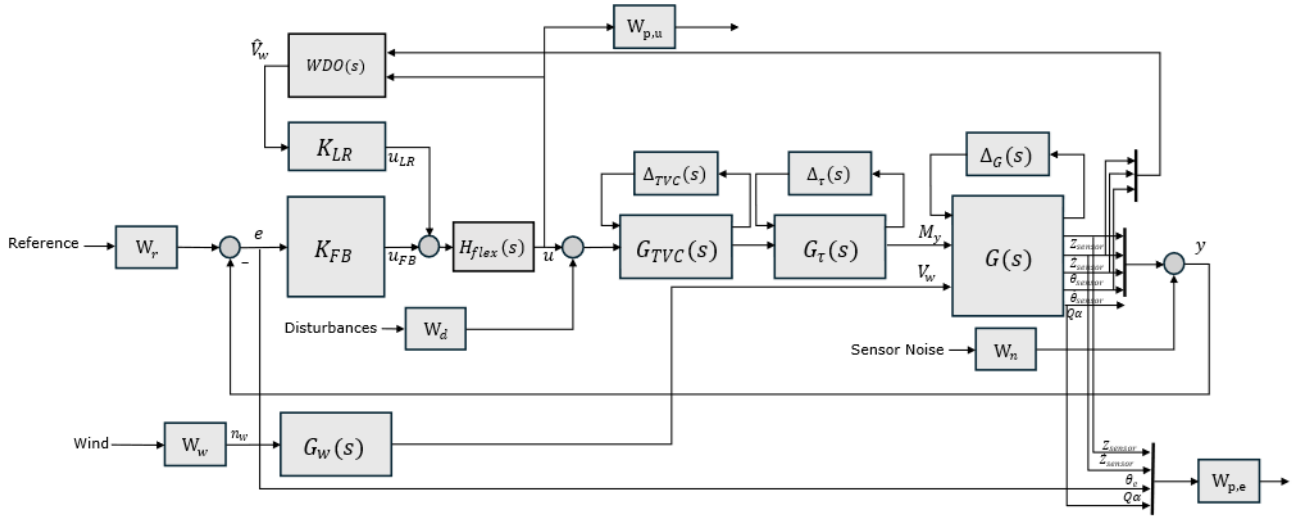

Fig. 8: Controller synthesis interconnection diagram for the pitch channel

A total of 4 mechanisms need to be designed [8]: a **Feedback Controller K_{FB}**, a **Flexible Filter $H_{flex}(s)$**, a **Load Relief Controller** K_{LR} and, finally and most importantly, the **Wind Disturbance Observer $WDO(s)$**, illustrated in figure 8. In the same figure, one can also find:

- $G(s)$: LTI plant corresponding to the uncoupled dynamics of the pitch channel and corresponding uncertainties, $\Delta_G(s)$.
- $G_\tau(s)$: block that model all the possible delays in the system and corresponding uncertainties $\Delta_\tau(s)$. It is implemented as a first order Padé approximation.
- $G_{TVC}(s)$: block that models the TVC dynamics with corresponding uncertainties, $\Delta_{TVC}(s)$, corresponding to a second order low-pass filter.
- $G_W(s)$: wind model corresponding to a second order Dryden filter.
- K_{FB}: feedback-only controller applied to the drift, drift rate, pitch and pitch rate errors.
- $H_{flex}(s)$: flexible filter designed to attenuate the control actuation at the flexible frequencies.
- K_{LR}: estimated wind feedback gain for LR. As described in the figure, the input of K_{LR} is obtained from the WDO [9].

- $W_{in} = diag(W_r, W_n, W_d, W_w), W_p = blkdiag(W_{p,e}(s), W_{p,u})$: input and performance weighting functions to impose the design specifications.

The feedback controller K_{FB} and flexible filter H_{flex} were designed first using a robust H_∞ approach, to obtain a stable and robust closed-loop.

Using the latter, the WDO was then designed to minimize the error between the actual wind disturbing the vehicle and the wind estimated by the WDO. More information about the design approach can be found in [8]. The work done in this SLE extends the work developed in [9] by also considering vehicle's flexibility, actuator saturation and delays, non-ideal state estimation and control discretization.

Figure 9 and 10 depict the drift rate, the attitude error, and the load $Q\alpha$ for the cases with and without load relief capability. The load relief capability allows one to reduce significantly not only the load but also the drift rate error, which are the physical quantities most affected by wind disturbances. In contrast, the attitude error increases as a consequence of the load relief capability, which was among the conclusions foreseen based on the work performed during the detailed design.

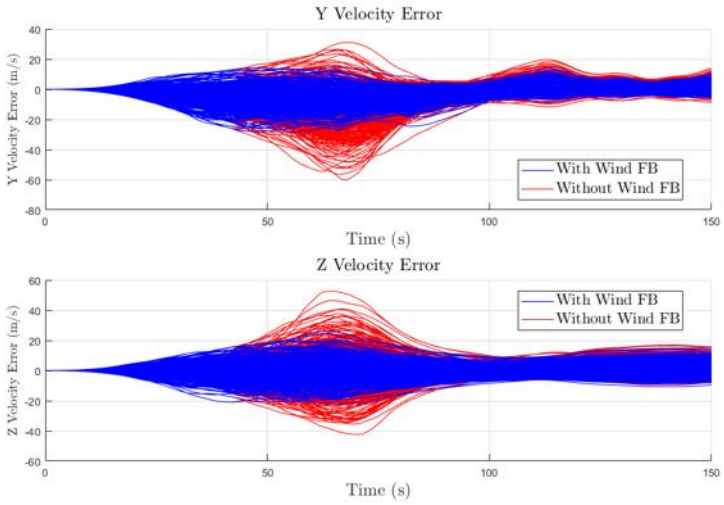

Fig. 9: Comparison of drift rate error between with vs without wind feedback

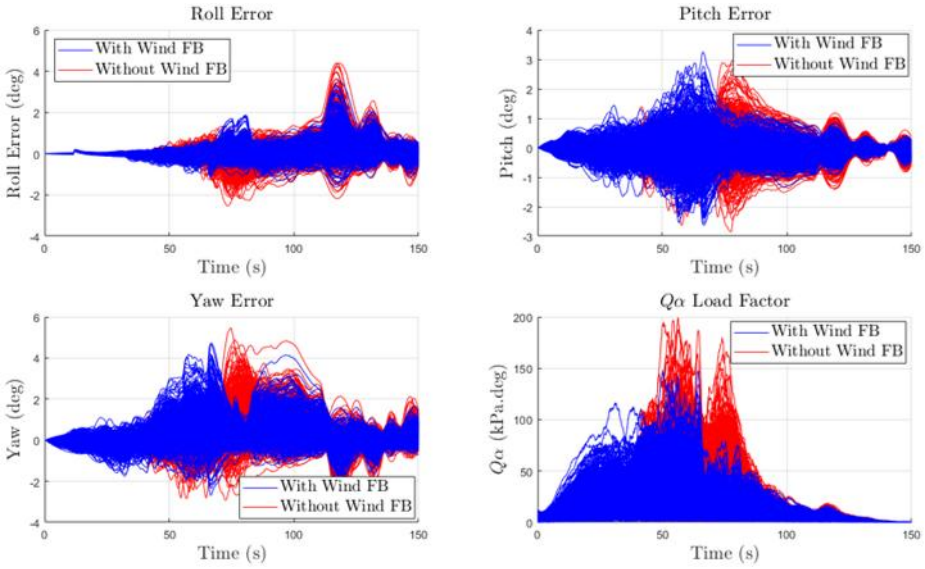

Fig. 10: Comparison of attitude error and load between with vs without wind feedback

The technology developed within SLE 4 improves launcher operations by:

- **Significantly decreasing the aerodynamic load** which the structures are subject to. A subsequent analysis showed that the average peak Qα load factor was reduced in 22%. Such achievement contributes to the **reuse, safety and reliability** of future launchers**.**
- Reducing the position dispersions at MECO, leading to a **more accurate payload injection into the target orbit.** The error between the target point and the actual position at MECO was reduced, on average, by 26.5%.
- **Increasing in the number of possible launch days/windows (higher launch frequency)**, as the impact of higher magnitude winds is attenuated. In fact, it was found that, without wind feedback and according to the previously defined load factor requirements, it was not possible to fly in 223 out of 365 days of the year, while, with the WDO, this number would be reduced to 75 days of the year. This implies that the **GNC solution developed within SLE 4 was able to more than double the number of possible launch days**.

Furthermore, other advantages of SLE 4 should be outlined:

- The possibility of **enabling/disabling the load relief capability** (and still maintaining robustness and performance guarantees) allows for higher flexibility of the technology.
- **Ease of verification**, given it was developed with state-of-practice tools that are well known and understood.
- **Reduced implementation cost**, since the control architecture does not require any extra sensors.
- **Enhanced mission planning flexibility** due to improved launch window availability.
- **Potential to reduce insurance and operational costs** through increased launch reliability.

Hence, the benefit of this technology outweighs the effort for its implementation, having no cost at all at H/W level.

3.3 Robust Safety Control

As further described in [10], SLE 11 addresses the topic of **safety** by employing **Control Barrier Functions (CBFs) [11][12]** as part of a **Safety Filter** that **augments the control architecture**. For this, the work started with the design of a **robust H_∞ baseline controller** applied to the ascent flight phase of a rigid launch vehicle. Secondly, a Safety Filter containing the CBFs was designed to limit the vehicle's drift from the reference trajectory within specified bounds, based on a robust formulation that accounts for unknown wind disturbances by assuming conservative bounds. During the design, it was identified some challenges related with stability, which led to the conclusion that there is a **trade-off between stability**

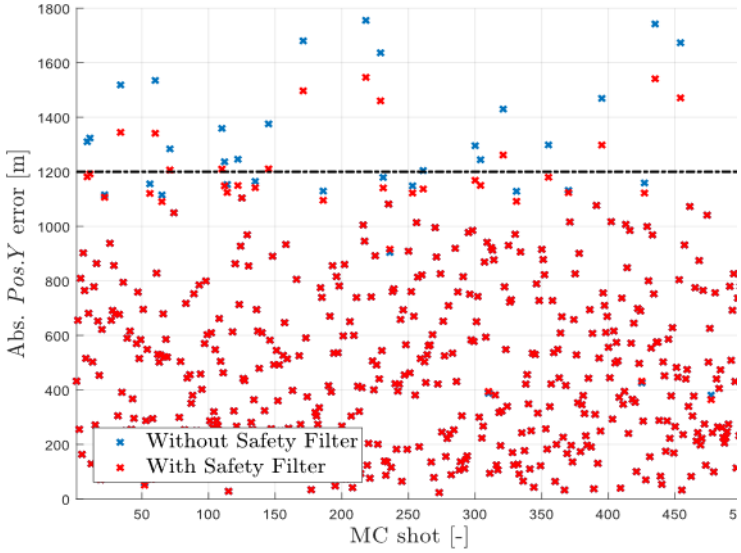

Fig. 11: Comparison of the maximum absolute drift per MC shot with vs without Safety Filter

and safety: when necessary, the Safety Filter with the CBFs overrides the baseline controller command in order to force the vehicle to remain within the safety drift bounds which leads, in several cases, to the increase of the attitude error that may lead to stability issues. This trade-off was tackled by introducing a second set of CBFs to bound the attitude error. Finally, the Safety Filter with the two sets of CBFs was tuned to satisfy as much as possible the safety drift bounds, while maintaining the attitude error bounds as large as possible to keep the vehicle stable. It is also remarked that an **Active-Set based solver has been developed in SURE** to solve the CBF optimization problem in an **efficient and fast manner**, while also satisfying the autocoding guidelines. This is important since the SLE was also tested in **SIL**, **demonstrating the feasibility of such technique to be executed in an onboard fashion**.

Figure 11 illustrates the maximum drift per MC shot obtained without and with the Safety Filter with both CBFs, in which it is possible to observe that the **Safety Filter is active when the vehicle is close to the boundary** and it reduces its violation to the extend permitted by the stability safety trade-off. Overall, the introduction of the Safety Filter decreases the number of cases that violate the drift error requirement from 20 to 12, which translates to a reduction of 40%.

At system-level, SLE 11 allows one to:

- Directly act on the safety of the launch vehicle, **increasing safety confidence**. It can improve the monitoring capabilities thereby helping operators take informed decision for the **flight termination. Additionally, the same monitoring capabilities can be useful for Autonomous Guidance re-computation algorithms.**
- Contribute to a **simpler V&V procedure**, as safety and performance metrics are imposed by design.
- **Improve cost-effectiveness**, as the added complexity of GNC is offset by real-time safety improvements.
- May improve stakeholder confidence (customers, regulators) due to **higher safety margins**.

The **benefits of implementing such technology outweigh the cost**, as actively tackling safety in real-time compensates for the increased GNC complexity.

During the execution of the project, the SURE team took advantage of the fact that multiple SLEs were being developed at the same time and started to **combine the techniques between SLEs**. One of these combinations is the **augmentation of the Safety Filter** implementation **with the Wind Disturbance Observer (WDO) developed in SLE 4**.

This augmentation process replaces the large wind bounds used in SLE 11 nominal formulation by smaller ones together with the wind estimated by the WDO, which leads to an overall reduction of the magnitude of the wind term in the CBF formulation. This reduction, in turn, leads to a **significant reduction of the conservatism of the Safety Filter performance**, as illustrated in figure 12: for the cases in which the Safety Filter is active, the inclusion of the WDO in the formulation led to a performance that further reduces the drift when the bound is violated, while maintaining the impact of the Filter at minimum when the bound is not violated. In other words, **the reduction of conservatism by including the WDO in the formulation improves two aspects: 1) it further reduces the dispersion of the extreme cases and 2) allows the launcher to fly closer to the safety bound without the intervention of the Safety Filter.**

The technical capabilities of the developed combined Safety Filter + Wind Disturbance Observer technology are as follows:

- **Increased performance** and **enhanced robustness**, when compared with the original SF implementation.
- **Reduced conservatism.**

Additionally, this technology inherits the system-level impacts from SLE 4 and SLE 11 mentioned before, such as:

- **The WDO inclusion can be enabled/disabled without loss of robustness and performance guarantees**.
- **The WDO integration in real-time SW has a reduced cost**.
- **The Safety Filter allows one to tackle actively the safety constraints during flight at a relatively low cost**.
- **Improved resilience to unexpected atmospheric disturbances.**

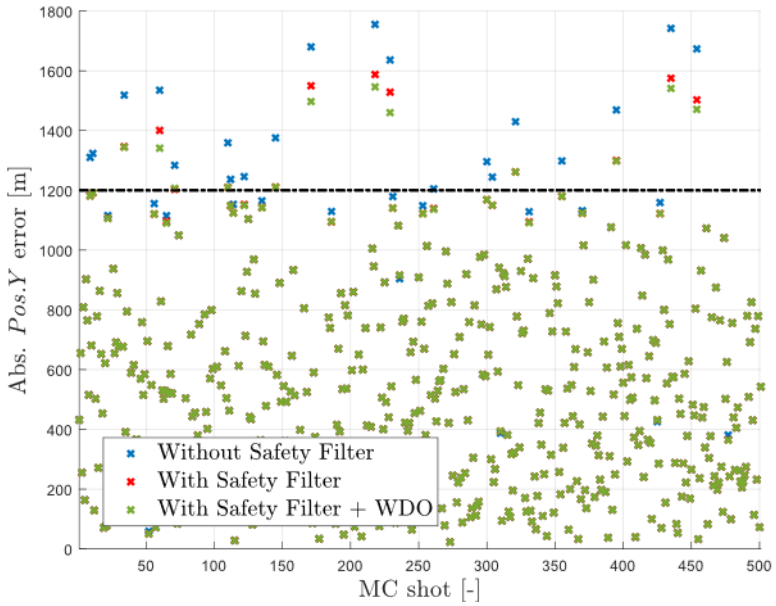

Fig. 12: Comparison of the maximum drift without Safety Filter vs with Safety Filter vs with Safety Filter and WDO

3.4 Robust control with Strain Sensors and Flexible Modes Reconstruction

The usage of **strain sensors**, Fiber Bragg Gatting (FBG) sensors in particular, for **flexible modes reconstruction** and advanced control was assessed. This may be used to counteract the structural vibrations and flexible characteristics of launch vehicles, allowing the manufacturers to increase their slenderness ratio and reduce their structural mass.

The FBGs are **distributed along the vehicle,** and the strain measurements are fed to the **Legendre polynomials-based deformation reconstruction method** proposed in [13], which requires previous knowledge of the modal shapes. The single-run results with perfect knowledge of the modal shapes are reported in figure 13.

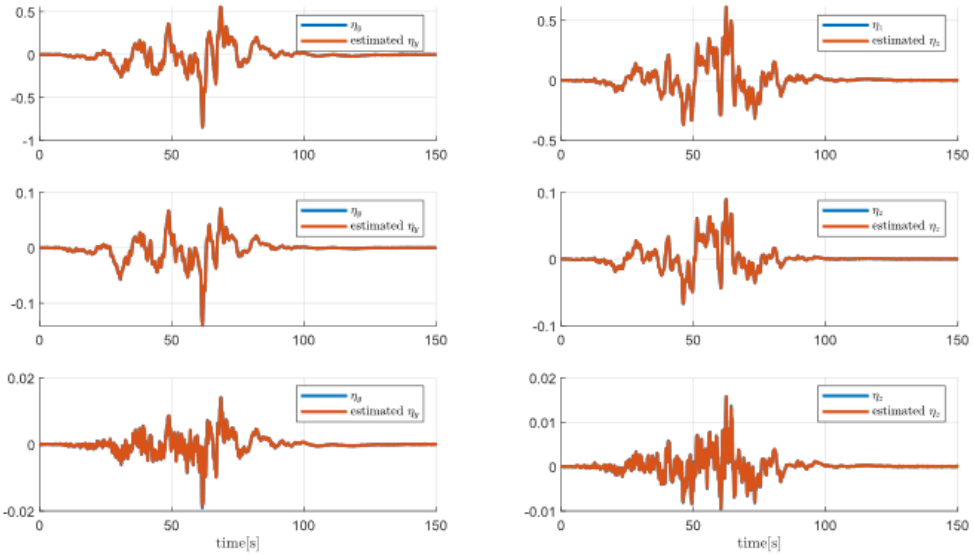

Fig. 13: True and estimated modal coordinates in ESA-i4GNC (framework developed in [3])

An analysis was done on the **number of strain sensors** to be mounted onboard the launch vehicle. As expected, as the number of sensors increases, so does the accuracy of the deformation reconstruction. The results show that **10 sensors per plane (x0y and x0z)** allow to have a **milimeter-level maximum error** in the estimated displacement. As such, 10 strain sensors were considered in the rest of the analysis.

The impact of **imperfect modal shapes knowledge** was assessed:

- First, the **lack of knowledge of higher order modes** was considered; assuming three as the total number of modes, the results show that with each higher order mode disregarded, the error increases by one order of magnitude.
- Then, the impact of **imperfect knowledge of the modal shapes themselves** was assessed: to emulate this uncertainty, each FBG location is dispersed randomly by ±5cm around its nominal location, as known by the navigation function; the worst-case error increases from 0.060 mm to 0.135 mm when the errors in the knowledge of the modal shapes are introduced.

An assessment of the **estimation of the time derivative of the modal coordinates** led to the conclusion that the main source of error is the fact that the time derivative computation is based on the current and past measurements, making it centred at **half a timestep** in the past, which corresponds to a 10 ms **delay**. Decreasing the time step comes at the cost of lower noise attenuation from the down sampling of the strain sensor measurements, which can be overcome with a low pass-filter that in turn adds a delay. As such, the deformation reconstruction frequency is kept at 50 Hz.

To conclude the assessment of the inclusion of strain sensors onboard a launch vehicle for deformation reconstruction, a **sensitivity analysis on the strain sensors performance model parameters** was conducted. The maximum delay considered, corresponding to one navigation timestep, increases the maximum y-displacement estimation error by one order the magnitude. Regarding the noise magnitude, each time it is increased by one order of magnitude, so does the maximum y-displacement estimation error. It is remarked that considering a zero delay or a zero-noise magnitude has a very small impact on the navigation estimate w.r.t. the baseline.

As mentioned before, in the spirit of combining different techniques developed during SURE, the implementation of the strain sensors and, in particular, the development of the flexible modes' reconstruction technique presented in the previous section inspired the augmentation of the feedback-only control architecture done in SLE 4 with the addition of the feedback of the flexible states, which

leads to the architecture depicted in figure 14 where K_{flex} corresponds to proportional gains applied to the estimated flexible estates $\eta_i, i = 1,2,3$.

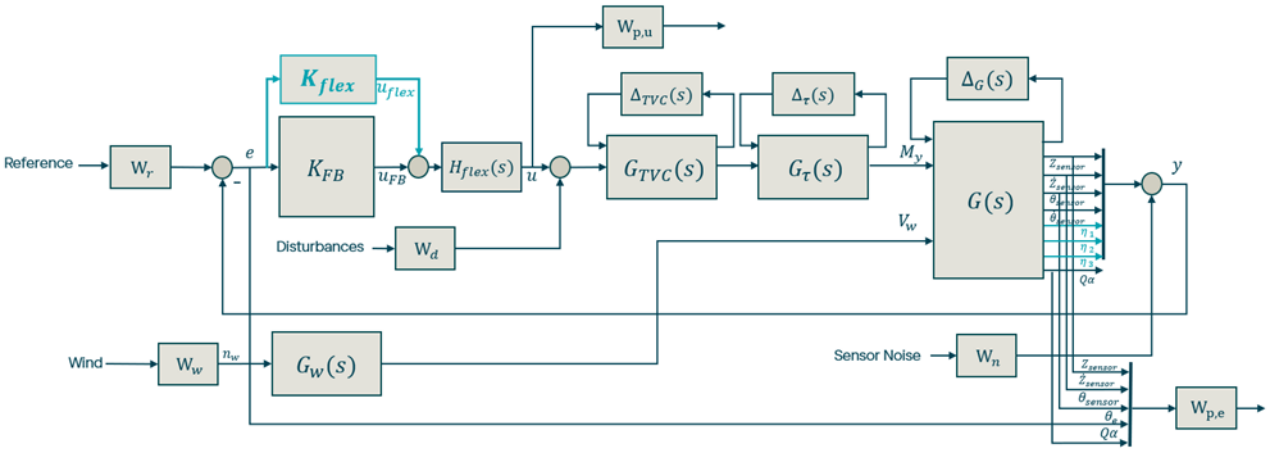

Fig. 14: Closed-loop diagram including flexible states feedback

Given this control structure augmentation, the design complexity is increased. In particular regarding the design choice for the flexible filter, $H_{flex}(s)$, composed by six notch filters, $H_{n,k}(s)$, and a low pass filter, $H_{LP}(s)$ [8]:

$$H_{flex}(s) = \left(\prod_{k=1}^{6} H_{n,k}(s)\right) \cdot H_{LP}(s),$$

$$H_{n,k}(s) = \frac{s^2 + \zeta_k s + \omega_k^2}{s^2 + \frac{\zeta_k}{\varepsilon_k} s + \omega_k^2}$$

$$H_{LP}(s) = \frac{\varepsilon_{LP} s^2 + \zeta_{LP} s + \omega_{LP}^2}{s^2 + \zeta_{LP} s + \omega_{LP}^2}$$

where:

- ω_k: frequency to be attenuated by the notch filter k
- ζ_k: width of the notch filter k
- ε_k: magnitude of attenuation of the notch filter k
- ω_{LP}: cut-off frequency of the low-pass filter
- ζ_{LP}: quality factor of the low-pass filter
- ε_{LP}: magnitude of attenuation of the low-pass filter.

for which three different design options were considered:

1. Option 1: $0 \leq \varepsilon_k \leq 1$ for $k = 1, \ldots, 6$: tune all the $\varepsilon_k$parameters with relaxed constraints. Note that for ε_k=1, the k notch filter is equal to the identity and, thus, it has no impact on the closed-loop. The filter obtained in section 3.2 is used as initialization.
2. Option 2: maintain the limits previously defined for the flexible filter and using the filter obtained in section 3.2 as initialization
3. Option 3: fixe the flexible filter parameters to the values obtained in section 3.2

The goal with this analysis is to better understand the need of the flexible filter in the closed-loop in an architecture where the flexible states are also being feedback. This process was repeated by also including the feedback of the flexible derivatives.

A key outcome of the design process was the confirmation that the **inclusion of the flexible filter** within the closed-loop architecture **remains essential to ensure robustness** against plant parameter uncertainties, **even when feedback from the flexible derivative** states is incorporated. In addition, the feedback of the flexible states leads to an increased actuation at the bending modes frequency which, if not properly handled, can drive the TVC deflection angles and rates into saturation.

Another important conclusion is that the **feedback of the flexible states is able to reduce the attitude error by reducing the peak of the sensitivity function (as illustrated in figure 15)**: this conclusion alone is sufficient to **support the continuation of the study proposed in this section**.

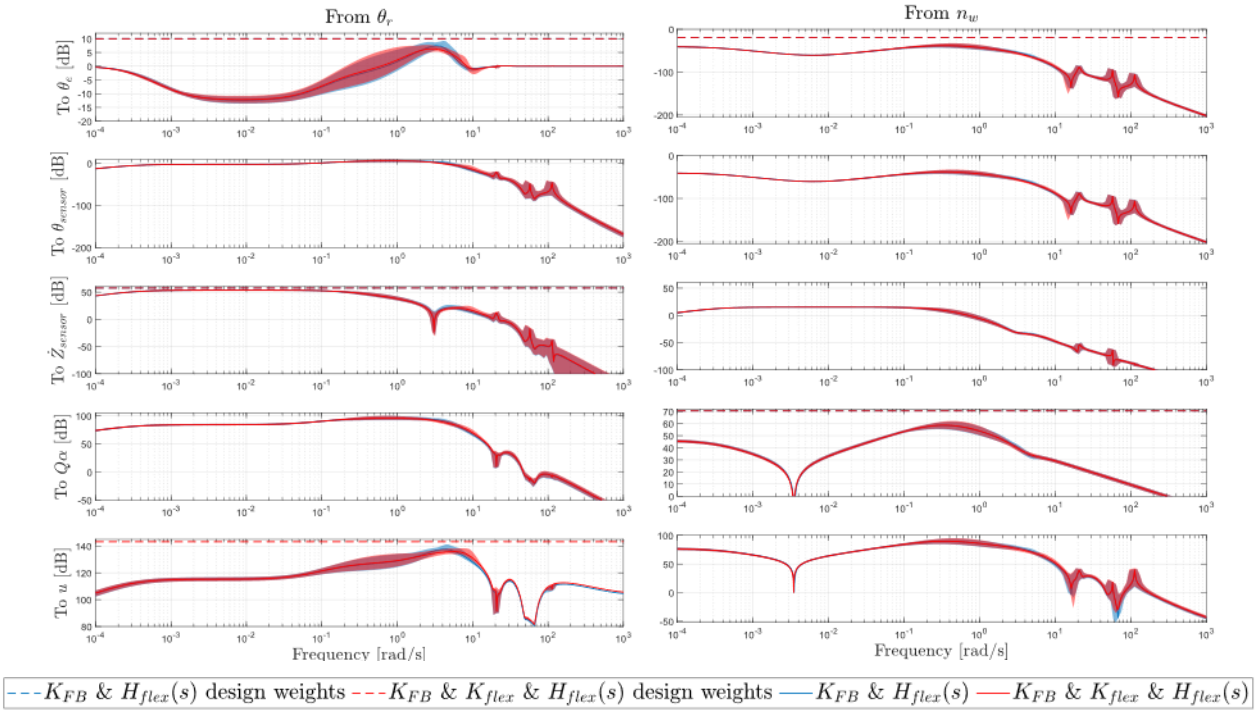

Fig. 15: Uncertain closed-loop transfer functions from pitch reference and wind noise to the performance outputs for t = 60 s. Closed-loop without (in blue) and with (in red) flexible states feedback

In conclusion, the considered implementation of strain sensors and subsequent flexible modes reconstruction allows the possibility to feedback the flexible information through the controller, as it is described above, and to correct the state estimated by the navigation, which is also affected by the flexible dynamics. In this sense, the combination of strain sensors, flexible modes reconstruction and flexible state feedback controller technologies mentioned above contribute to:

- **Potential improvement of structural health monitoring**, detecting early signs of fatigue or anomalies.
- **Mitigate the flexibility impacts on closed-loop performance** by allowing the controller to actively counteract flexible mode dynamics. However, actuation at flexible mode frequencies may be limited by actuator saturation.
- **Increase the fuel efficiency by allowing to design slender and more flexible vehicles.** By reducing the impact of flexibility on the closed-loop, it becomes possible to further decrease the vehicle's mass/weight which, in turn, increases its flexibility.
- **Facilitates scalability of the control system design approach** to larger or more flexible launch vehicles.

4 Conclusions

The SURE project has delivered a **comprehensive and in-depth exploration of advanced GNC (Guidance, Navigation, and Control) techniques for launch vehicles**. Through a structured and methodical approach, the project has significantly contributed to the current state of knowledge in this domain.

From an extensive initial review of the state-of-the-art to the selection, development, and validation of multiple **Smart Launcher Enablers (SLEs)**, SURE has demonstrated the feasibility, performance, and potential of several **innovative GNC solutions**. These were tested in high-fidelity simulation environments, covering both ascent and landing scenarios, and verified through rigorous **MIL and SIL testing**. These results confirm that the techniques developed within SURE are both technically sound and have strong potential for further development and integration into future launcher systems.

Acknowledgments

The results presented in this paper have been achieved under the SURE project. The SURE project is funded by the European Space Agency through Contract No. 4000142645/23/NL/CRS. The views expressed in this paper can in no way be taken to reflect the official opinion of the European Space Agency.

Declaration of Use of Artificial Intelligence

Artificial intelligence was not used in the work presented.

References

[1] Final Report, “Autonomous MVM and Monitoring Systems for Safe and Adaptable Launcher GNC Systems”, ESA Contract 4000142645/23/NL/CRS

[2] A. Marwege and A. Guelhan and J. Klevanski and C. Hantz and S. Karl and M. Laureti and G. De Zaiacomo and J. Vos and M. Jevons and C. Thies and A. Krammer and M. Lichtenberger and J. Carvalho and S. Paixão, “RETALT: review of technologies and overview of design changes”. Space Journal, Springer, 2022, DOI: 10.1007/s12567-022-00458-9

[3] Final Report, Artificial Intelligence techniques for GNC design, implementation and verification, ESA Contract 4000134108/21/NL/CRS

[4] D. Malyuta et al., "Convex Optimization for Trajectory Generation: A Tutorial on Generating Dynamically Feasible Trajectories Reliably and Efficiently," in IEEE Control Systems Magazine, vol. 42, no. 5, pp. 40-113, Oct. 2022, doi: 10.1109/MCS.2022.3187542

[5] M. Sagliano et al., “Powered Atmospheric Landing Guidance for Reusable Rockets: the CALLISTO studies,” AIAA SCITECH 2024 Forum, DOI: 10.2514/6.2024-1761.

[6] Y. Yu, P. Elango, B. Açıkmeşe and U. Topcu, "Extrapolated Proportional-Integral Projected Gradient Method for Conic Optimization," in IEEE Control Systems Letters, vol. 7, pp. 73-78, 2023, DOI: 10.1109/LCSYS.2022.3186647

[7] A. Domahidi, E. Chu and S. Boyd, "ECOS: An SOCP solver for embedded systems," *2013 European Control Conference (ECC)*, Zurich, Switzerland, 2013, pp. 3071-3076, doi: 10.23919/ECC.2013.6669541.

[8] J. P. Belfo, B. Ribeiro, G. Videira, A. Botelho, I. Zagalo, P. Guerreiro, A. Montero Miñán, J. Vasconcelos, P. Rosa, Adolfo D. Silva, P. Simplício, M. Casasco. "Robust Wind Disturbance Observer Design for a Flexible Launch Vehicle".11th Symposium on Robust Control Design, ROCOND 2025, Porto, Portugal.

[9] Simplício, P., Marcos, A., and Bennani, S. (2021). Launcher flight control design using robust wind disturbance observation. Acta Astronautica, 186 303-318. DOI: 10.1016/j.actaastro.2021.05.044.

[10] Aitor Gomez, J. Belfo, P. Rosa, P. Simplício, Jakob Stoustrup. "Safety Filter for Rocket Thrust Vector Control: Monitoring and Enforcing Flight-Envelope Constraints", EuroGNC 2026, DOI: 10.82124/CEAS-GNC-2026-090.

[11] R. Wisniewski and M. L. Bujorianu. Safety of stochastic systems: An analytic and computational approach. Automatica, 2021.

[12] Ames, A.D., Coogan, S., Egerstedt, M., Notomista, G., Sreenath, K., Tabuada, P., 2019. Control Barrier Functions: Theory and Applications.

[13] Zhuang, Liang, and Zhang Yulin. "Deformation Reconstruction and High-Precision Attitude Control of a Launch Vehicle Based on Strain Measurements." International Journal of Aerospace Engineering, vol. 2021, 6 Feb. 2021, pp. 1–20, https://doi.org/10.1155/2021/6672943.